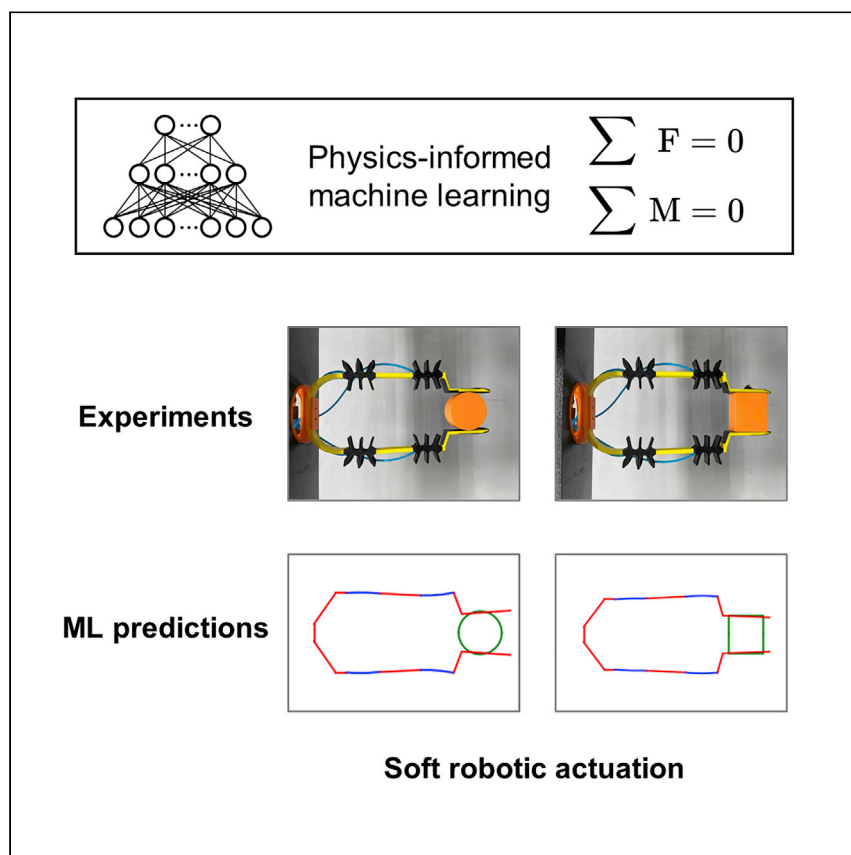


Article

Efficient pneumatic actuation modeling using hybrid physics-based and data-driven framework



Zhizhou Zhang, Zeqing Jin,
Grace X. Gu

ggu@berkeley.edu

Highlights

Neural network models are trained to capture the mechanics of pneumatic actuators

Pneumatic behavior is predicted by minimizing unbalanced forces and torques

Combining data and physics knowledge reduce prediction and training time

Prediction can be improved by adding regularization terms and historical dependency

Zhang et al. present an efficient predictor for pneumatic actuation utilizing a combination of data-driven surrogate modeling and physics-based optimization. This hybrid methodology can explicitly capture the nonlinear mechanics of pneumatic components for robotic devices with soft actuation.

Zhang et al., Cell Reports Physical Science 3,
100842
April 20, 2022 © 2022
<https://doi.org/10.1016/j.xcrp.2022.100842>



Article

Efficient pneumatic actuation modeling using hybrid physics-based and data-driven framework

Zhizhou Zhang,¹ Zeqing Jin,¹ and Grace X. Gu^{1,2,*}

SUMMARY

Soft robotics, characterized by structural compliance, offers advantages when handling fragile objects and interacting with humans. Modeling the mechanical behavior of soft robots, however, is often overlooked in previous studies due to the difficulty of capturing their nonlinear deformation. In this work, we present a highly efficient predictor for pneumatic actuation utilizing a combination of data-driven surrogate modeling and physics-based optimization. This hybrid methodology explicitly captures the nonlinear mechanics of pneumatic components, which greatly accelerates the searching of static equilibrium, and thus help elucidate how the overall grasping system will interact with the environment. We have additively manufactured and tested a robotic device on various objects. Results show that our model can predict pneumatic actuation very closely matching to that of the experiments with orders of magnitude faster computational speed than traditional numerical simulations. Moreover, the proposed framework can be extended to model various soft robotic devices with nonlinear actuation components.

INTRODUCTION

Robotics has been an exponentially growing research field for decades and can generally be divided into two main categories: hard robots and soft robots.¹ Aply named, hard robots typically have chains of rigidly hinged links that are made up of materials with modulus values of 10^0 – 10^3 GPa.^{2,3} The hard robotics field is highly developed and successful in conducting various sophisticated tasks requiring large force output, fast response, and precise control.^{4,5} However, rigid structures have intrinsic shortcomings, increasing research interest in soft robotics. Soft robotics introduce structural compliance by either using soft materials directly (within a modulus range of 10^{-2} – 10^3 MPa) or using actuators with controllable resistance, creating two major advantages: more reliable handling of fragile objects and safer interactions with humans and environments.^{6–9} Such characteristics enable a wide range of applications, including rescue robots, biomedical devices, prosthetic hands, packaging of goods, among others.^{10–13} Soft robotics are typically driven by one of the following actuation mechanisms: pressure (pneumatic or fluidic),^{14,15} tendon,^{16,17} or smart responsive polymers,^{18–20} among which pneumatic actuation has received the most attention for its design flexibility and ease of operation. Over the past decade, the design of pneumatically actuated soft robots has been extensively studied to achieve different deformation profiles, such as bending, twisting, and lengthening.^{21,22} Meanwhile, researchers have also developed a variety of fabrication techniques for pneumatic actuators including 3D printing, soft lithography, and injection molding.^{3,23–26}

¹Department of Mechanical Engineering, University of California, Berkeley, CA 94720, USA

²Lead contact

*Correspondence: ggu@berkeley.edu

<https://doi.org/10.1016/j.xcrp.2022.100842>



Despite the thorough understanding in the design and manufacturing of pneumatically actuated soft robots, there has been a lack of research in modeling their mechanical behavior. Numerous simulators have been developed to model the behaviors of hard robots accurately and efficiently,^{27–29} which serve as the basis for various rigid body dynamics control research.^{30,31} However, similar approaches are not adaptable to pneumatic (soft) robots due to their structural compliance. Accurately predicting the deformation of a pneumatic actuator or robot requires the detailed strain field, which is typically computed using numerical tools, such as finite element method (FEM). Unfortunately, such pure physics-based method as FEM is computationally intensive, making it infeasible for making fast predictions. As a result, most research on pneumatic actuators use FEM to sweep a parametric design space or merely as a demonstration tool.^{32–34} Few studies have mathematically modeled the deformation behaviors of pneumatic actuators based on geometry or loading simplifications, such as constant total length, constant curvature, soft elastic beam assumptions, zero loading, or unidirectional loading.^{35–37} These studies show promising results when predicting the kinetics and kinematics of a single pneumatic actuator or joint, but are not well examined when functioning as a component of a gripper system that involves more complex loadings. This underscores an important research gap in general-purpose efficient modeling for pneumatic actuators and grippers.

Previously, we designed a pneumatic actuator where its bellow structure is optimized for dexterity under given pressure inputs.³⁴ A pneumatic gripper is then constructed using the designed actuator that functions as the joints. The gripper is expected to stay in the 2D vertical plane with the two fingers operating symmetrically, where each finger contains four pressure control channels. Unlike most existing designs, which have the pneumatic actuator functioning as the entire finger,^{38–40} the proposed articulation allows more flexibility in gripper configuration and operation. The goal of this paper is to establish a static predictor (Figure 1A) that models the pneumatic gripper gesture accurately and more efficiently than FEM. More specifically here, gesture refers to the spatial location, orientation, and deformation of each pneumatic gripper component, which we hope to predict from the input pressures and the object to be held as seen in Figure 1B. Recently, advances in machine learning methods such as neural networks (NNs) allow for an efficient analysis of various material systems.^{41–47} However, a direct supervised learning on ground truth gestures requires full gripper simulations, which is computationally expensive and lacks generalizability. Instead, NN supervision only serves as a data-driven explicit approximation to the implicit nonlinear mechanics of the pneumatic actuators (joints), using FEM results under random loading conditions. This approach is alternatively named as surrogate modeling, which has been successful in various tasks that require accelerated numerical simulations.^{48–51} The joint surrogate model serves as a solution space for all physically viable pneumatic gripper gestures. The entire gripper gesture prediction is then achieved under a data-free scheme through searching for the optimal solution over the trained surrogate model to satisfy static mechanics and contact constraints that are physics prior knowledge. As a result, the gripper modeling framework is hybrid, which includes a physics-based loss function, and nonlinear constraints formed by the data-driven pneumatic joint surrogate model. Two potential routes are explored for the gesture modeling, an implicit iterative solver, which minimizes the system unbalance under certain pressure inputs, and an NN approach that directly maps the pressure control space to the pneumatic joint operating space using physics loss. In other words, the NN approach will be supervised by static equilibrium balance (physics loss) rather than ground truth gesture data. Both methods can accurately predict gravity's effect on pneumatic gripper

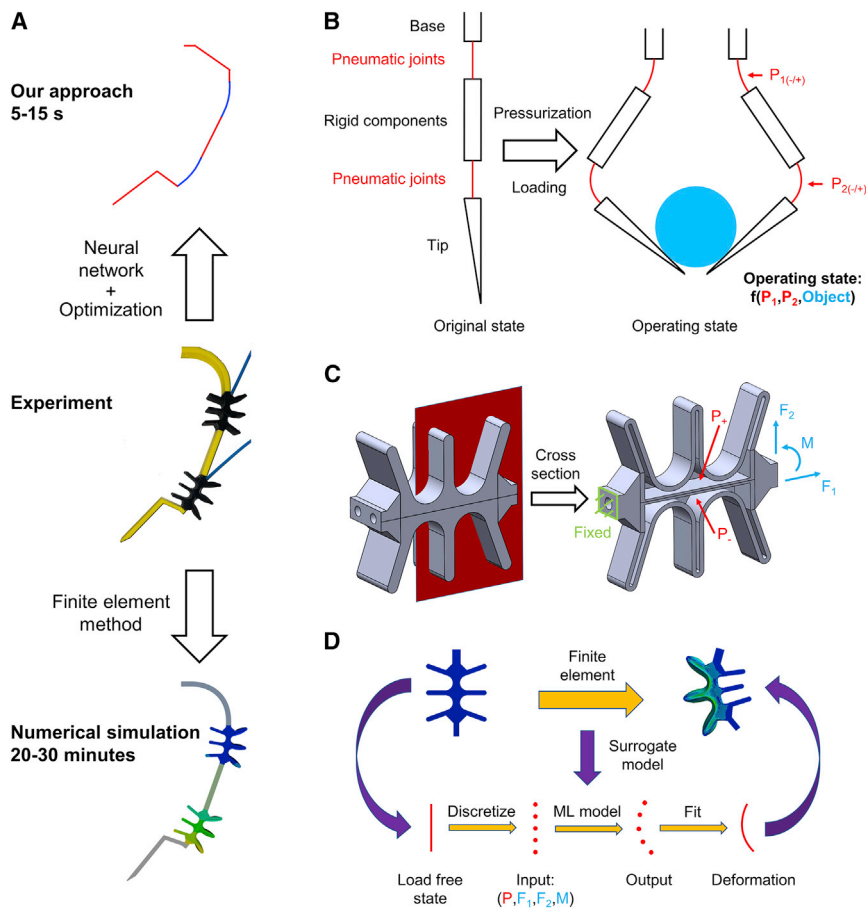


Figure 1. The efficient gesture predictor for a 3D printed pneumatic gripper

(A) Utilizing the power of neural network surrogate modeling and nonlinear optimization, an efficient predictor is established to shorten the computation time by orders of magnitudes compared with classical numerical simulation approaches.

(B) A 2D schematic of the pneumatic gripper is constructed whereby the deformed joints are represented by their center lines. The pressure control is represented as P_1 and P_2 with positive and negative values corresponding to the right and left channels, respectively.

(C) The cross-section view of the pneumatic joint CAD model. In the FEA simulation, the joint is considered to be fixed at the proximal end and loaded at the distal end. The coordinate of the force is consistent with the undeformed joint coordinate. The input pressure is defined as positive when the top bellow channel is pressurized, and vice versa.

(D) The schematic for the joint surrogate model. The surrogate model (neural network) takes the pressure, forces, and torque as inputs and predicts the deformed coordinates of 10 anchor points on the joint center line.

gestures with greatly reduced computation time. When estimating the object gripping gestures, there remain unsolved challenges that impede the forward NN predictor from properly learning the contact states, making instantaneous gesture estimations difficult. However, the inverse iterative solver built upon the joint surrogate model still shows good performance and has shortened the computation cost by orders of magnitude compared with numerical methods.

RESULTS

Joint surrogate modeling

To realize fast gesture prediction for a soft gripper, the first step is to construct the solution space by establishing a differentiable forward model for the nonlinear

component (pneumatic joint) of the gripper. This is achieved through a surrogate model implemented using deep NNs based on numerical simulation results. For the most generality, the loading and boundary conditions applied on the pneumatic joint are agnostic of the entire gripper assembly so that the surrogate model is consistent regardless of the joint location. The deformation of the joint is determined by pressure in the channel, force, and torque applied at the distal end of the joint; hence these five parameters (two pressure values, the joint end tangential and normal forces, and one torque value) are considered as input features to the NN (Figure 1C). To simplify the input features, we use one parameter to represent the pressure state of the joint since there is always one channel kept at ambient pressure. We assign the positive range of the pressure parameter to the upper pneumatic channel and the negative range to the lower pneumatic channel as seen in Figure 1C. In this way, four parameters (P , F_1 , F_2 , and M) are left and serve as inputs to the surrogate model. The range of the input parameters are set to be $0 \leq P \leq 0.3$ MPa, $-3 \leq F_1 \leq 3$ N, $-3 \leq F_2 \leq 3$ N, and $-0.1 \leq M \leq 0.1$ Nm. The output of the model contains the position vectors of 10 equally distanced anchor points on the center line (Figure 1D) with respect to the proximal end of the pneumatic joint, denoted as $r_i = [x_i, y_i]^T$, $i = 1, 2, \dots, 10$. The surrogate model is then written as $R = \text{sur}(P, \tau)$, where $R = [r_1, r_2, \dots, r_{10}]$ and $\tau = [F_1, F_2, M]^T$. The function $\text{sur}(\cdot)$ is realized through a deep NN which is fine-tuned on the number of layers as well as nodes to achieve optimal performance (Figure 2A). The training data were obtained from FEM simulation based on randomly generated input variables. A total of 2,560 sets of simulated joint deformation is obtained and divided into training, validation, and testing dataset with a 7:2:1 ratio, respectively. The FEM simulation for a single pneumatic joint takes approximately 7 min to accomplish. Taking advantage of the symmetry of the pneumatic joint, each training data tuple $\{R, P, \tau\}$ can be augmented to create new data $\{R \cdot [1, -1]^T, -P, \tau \cdot [1, -1]^T\}$. The Adam optimizer is used with a learning rate of 0.0016 and an exponential rate factor of 0.99/epoch to conduct gradient descent. The training result on the original and augmented training datasets is shown in Figure 2B. The loss is defined as the average error (Euclidean metric) between predicted coordinates r_i and the ground truth \tilde{r}_i (coordinates obtained from simulation) over the 10 anchor points, denoted as $\frac{1}{10} \sum_{i=1}^{10} \|r_i - \tilde{r}_i\|$. The augmented dataset reaches a loss value of 0.19 mm after 500 epochs of training. As the length of the joint is 45.45 mm, the average loss achieved by our surrogate model is less than 0.5% of the joint size. Figure 2C shows a comparison between FEM simulations and surrogate model predictions on two randomly selected cases. The color bar in the FEA simulation result represents the amount of total displacement. The surrogate model prediction is visualized as a plain red color, which matches well with the numerical simulations. As a baseline comparison, a k-nearest neighbors (KNNs) regression model is constructed on the same dataset with $k = 4$ determined from validation. Despite the low input dimension, the KNN model shows an average loss of 1.04 mm (~ 5 times of the NN loss), confirming the necessity of interpolating the pneumatic joint behavior with an NN. Furthermore, the auto differentiation ability of the NN offers fast gradient computation, which is essential for finding the equilibrium gripper gesture.

Error propagation of the surrogate model

To describe the gesture of the gripper using only the anchor points on the center line of the pneumatic joints, one important assumption made is that the pneumatic joints and the rigid components are tangent to each other at their connections. Based on this assumption, the orientation at the end of a pneumatic joint is determined as $\varphi_i = \theta_i + \cos^{-1} \frac{(r_{10} - r_9) \cdot e_x}{r_{10} - r_9}$, where φ_i and θ_i represent the orientation at the distal and proximal end of joint i (index shown in Figure 1B). Note that θ_2 and φ_1

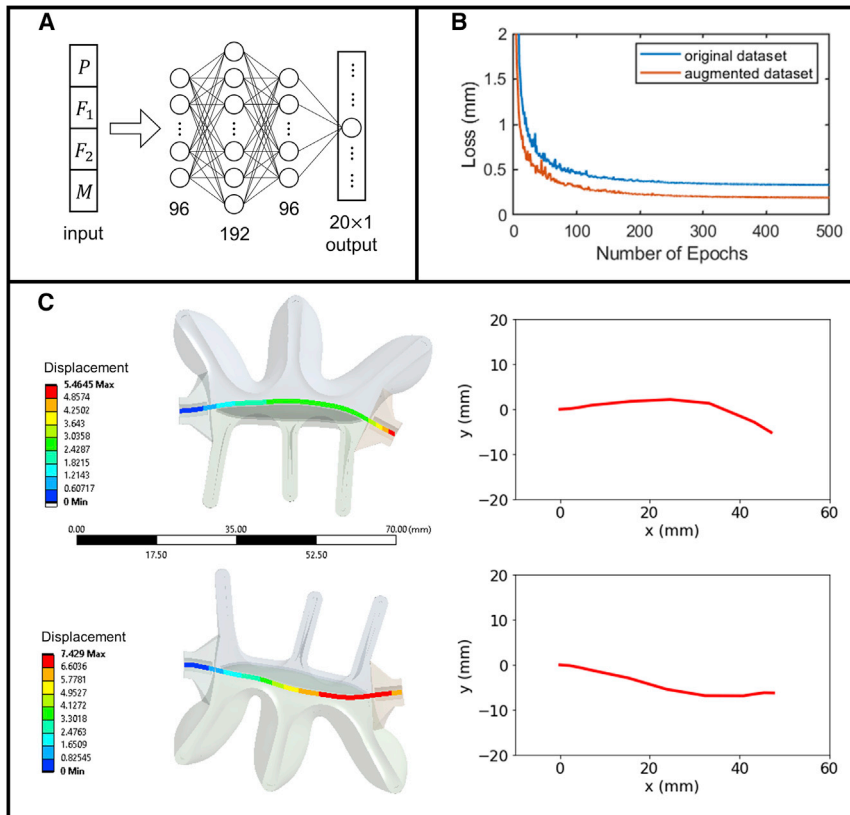


Figure 2. Sample predictions from the joint surrogate model

(A) Neural network structure of the joint surrogate model. The model takes pressure, force, torque states as inputs and outputs the displacement of the 10 anchor points on the joint center line in the 2D plane. The neural network contains three hidden layers of sizes 96, 192, and 96.

(B) The validation loss over the training process. The loss has a unit of millimeter and represents the distance from the predicted coordinates to the ground truth coordinates. The symmetry augmented dataset has superior performance.

(C) Two random comparisons between the FEA simulation and surrogate model predictions. The FEA results are shown on the left with the color bars showing the total displacement. The deformed joint centerline coordinates predicted by the surrogate model are plotted on the right. The top row has $p = 0.34$ MPa, $F_1 = 1.84$ N, $F_2 = 2.02$ N, $M = 2.73$ Nmm. The bottom row has $p = -0.3$ MPa, $F_1 = 2.97$ N, $F_2 = -2.35$ N, $M = -5.85$ Nmm.

are always equivalent since they are connected by a rigid rectangular part. As the number of joints increases (from a single joint to a gripper system), the deformation error accumulates and magnifies at the tip end. For instance, a 1° change for φ_1 would cause an approximately 3 mm displacement at the gripper tip. Therefore, it is important to investigate the performance of the joint surrogate model when assembled with rigid components. In Figure 3, four groups of pressure settings are compared among the results of FEA simulation, joint surrogate model, and experiments. At this stage, no kinetics is involved, and the gestures are purely results of pressurization. Among the output results, bending angle is one of the dominant factors that affect the gripper gesture and is highlighted and labeled in Figure 3. Taking the FEM simulation results (middle column in Figure 3) as a reference, the 3D printed gripper tends to bend less while the surrogate model tends to predict excessive bending as seen in Figure 3A and 3B. In this case, the two pneumatic joints are pressurized in the same direction. Although being insignificant on a single joint, the error accumulates and causes distinct predictions at the gripper tip. On the other

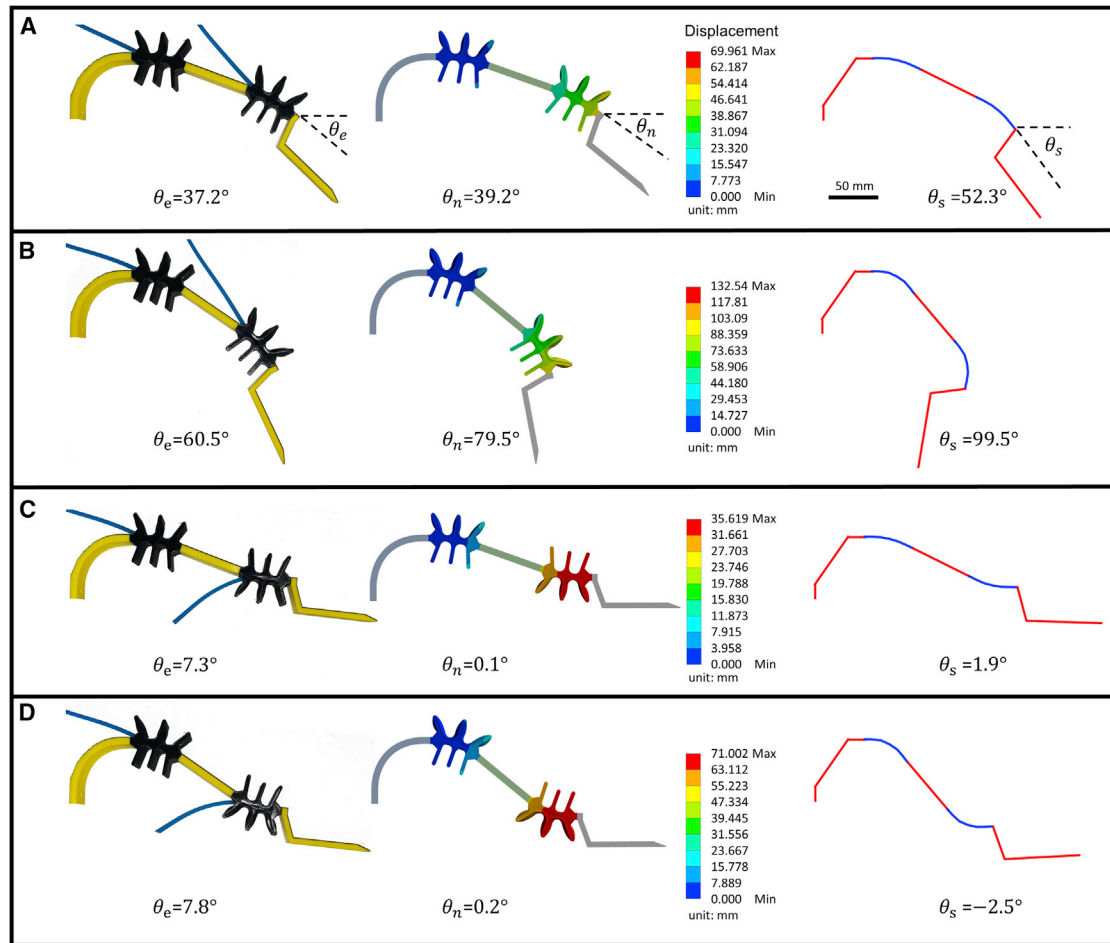


Figure 3. Error propagation of the surrogate model on the assembled gripper

(A–D) Comparison between the tip orientation obtained from experiments (θ_e), numerical simulations (θ_n), and the joint surrogate model (θ_s) on one of the entirely assembled gripper finger. The joints are pressurized to deform without constraints, and there are no forces or torques involved in this test. The color bars represent the amount of total displacement predicted by FEM. In the plots generated by the surrogate model, the red curves represent the rigid components and the blue curves represent the pneumatic joints.

(A) $p = 0.05$ MPa for both joints. (B) $p = 0.1$ MPa for both joints. (C) $p = 0.05$ MPa for joint 1, and $p = -0.05$ MPa for joint 2. (D) $p = 0.1$ MPa for joint 1, and $p = -0.1$ MPa for joint 2.

hand, when the two joints are pressurized oppositely as seen in Figures 3C and 3D, we obtain similar gripper tip rotations from experiments, FEM, and the surrogate model. In this case, the prediction error from the two joints compensates for each other. Nevertheless, excessive joint deformation predicted by the surrogate model yields a larger vertical displacement at the gripper tip. Although the error from the joint surrogate NN seems to accumulate and becomes non-negligible at the gripper tip, it is greatly mitigated when external forces and torques are involved, which will be discussed in more detail in the following sections.

Soft gripper gesture prediction

With the fine-tuned pneumatic joint surrogate model, we are ready to establish a predictor that models how the assembled pneumatic gripper will hold an object in the vertical plane. Due to the nonlinear correlation among the deformation, force, and torque states of the soft gripper, the modeling has to be realized implicitly. As seen in Figure 4A, the predictor takes the object information and the control

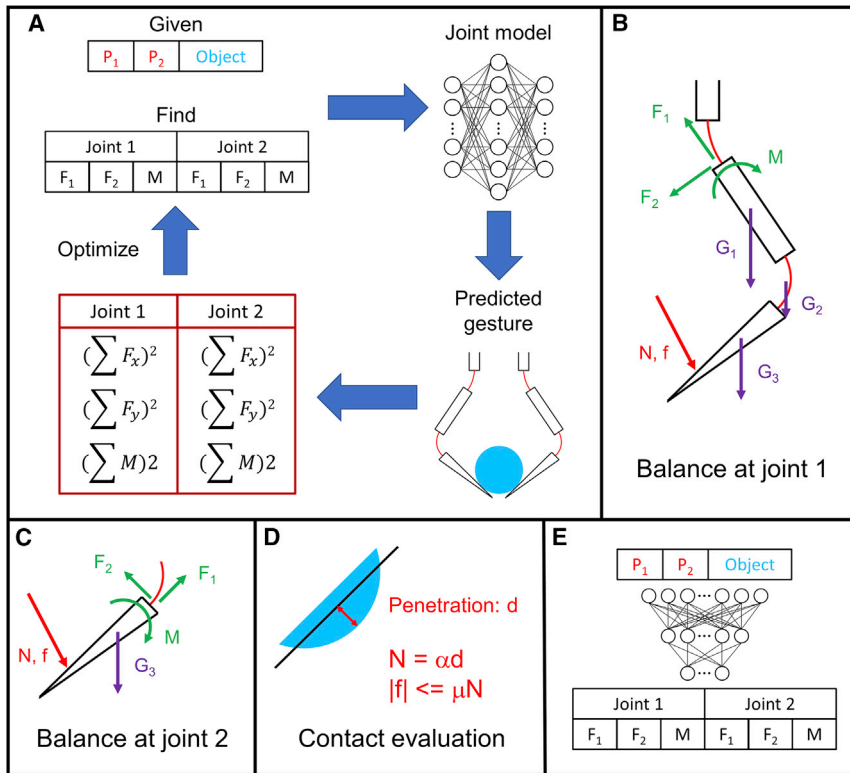


Figure 4. Methodology for efficient pneumatic gripper gesture predictor

(A) Schematic showing the gripper gesture solution process. The gesture is solved by optimizing the force and torque states at the two joints. Using the trained joint surrogate model, deformation of the entire gripper can be determined from the pressure, object information, and joint states. Based on the deformation, force, and torque balances at the two joints can be analyzed to construct the loss function, which is a differentiable function of the joint states. Joint states are then updated to minimize the loss.

(B) Forces and torques from joint 1 are balanced with the weight of the remaining gripper components and contact forces.

(C) Forces and torques from joint 2 are balanced with the weight of the tip and the contact forces.

(D) The normal contact force is evaluated through the penalty method. Friction depends on the weight of the object and is constrained by the friction cone.

(E) Alternatively, the gesture solving process can be replaced by a neural network model that directly maps the pressure inputs to corresponding joint states. In this case, the neural network parameters are optimized rather than the joint states.

signals (joint pressure inputs) as its inputs, and predicts the force and torque states $\tau_i = [F_1 \ F_2 \ M]_i^T$ at the pneumatic joints. In this work, we assume the object and the two gripper fingers are symmetrical so that only two pressure controls, P_1 and P_2 , are considered. The pressure inputs P_i and predictor outputs τ_i are then fed into the joint surrogate model, which computes the deformation of the pneumatic joints ($R_i = \text{sur}(P_i, \tau_i)$) and, therefore, the soft gripper gesture. Based on the current prediction, net force and torque are evaluated at the distal end of the two joints. More specifically, τ_i must be in balance with the weight of the corresponding gripper components and the contact forces as shown in Figures 4B and 4C. We apply the penalty method to calculate the normal contact force (N) whose magnitude is proportional to the penetration between the object and the gripper tip, as seen in Figures 4D and S1. The static friction (f) is determined by the weight of the object and constrained by the friction cone (more details in Note S1). The entire gripper gesture is then modeled by considering static equilibrium so that any nonzero net

force or torque residual is squared to become a physics-driven loss function L , which can be represented as Equation 1, where $F_x(\cdot)$, $F_y(\cdot)$, and $M(\cdot)$ are the transformed force and torques states in the global coordinate system (Equation 2), τ_c and φ_c represent the contact state, G_j is the weight, illustrated in Figures 4B and 4C, $M_{G_j} = (\hat{r}_{G_j} - \hat{r}_{10}) \times G_j$ is the torque generated by weight G_j with $\hat{r}_{G_2} = \frac{1}{10} \sum_k \hat{r}_k$ for joint 2, and α , β , and γ are tunable loss function parameters. The global positions $\hat{R}_i = [\hat{r}_1 \hat{r}_2 \dots \hat{r}_{10}]_i$ can be obtained from Equation 3 using the corresponding proximal end coordinate $r_{0,i}$ and orientation θ_i . Since the loss function is differentiable with respect to the joint force and torque states (i.e., the NN joint surrogate model can be backpropagated), gradient steps can be calculated to update τ_i and minimize the loss.

$$L = \sum_i \left[\alpha (F_x(\tau_i, \varphi_i) + F_x(\tau_c, \varphi_c))^2 + \beta \left(F_y(\tau_i, \varphi_i) + F_y(\tau_c, \varphi_c) + \sum_j G_j \cdot e_y \right)^2 + \gamma \left(M(\tau_i, \varphi_i) + \sum_j M_{G_j} \right)^2 \right] \quad (\text{Equation 1})$$

$$\begin{bmatrix} F_x \\ F_y \\ M \end{bmatrix} (\tau_i, \varphi_i) = \begin{bmatrix} \cos(\varphi_i) & -\sin(\varphi_i) & 0 \\ \sin(\varphi_i) & \cos(\varphi_i) & 0 \\ 0 & 0 & 1 \end{bmatrix} \tau_i \quad (\text{Equation 2})$$

$$\hat{R}_i = r_{0,i} + \begin{bmatrix} \cos(\theta_i) & -\sin(\theta_i) \\ \sin(\theta_i) & \cos(\theta_i) \end{bmatrix} R_i \quad (\text{Equation 3})$$

Besides the iterative gesture predictor, we also explore the possibility of establishing an NN as a direct model, as seen in Figure 4E. This NN approach adopts the exact same loss function as the iterative approach, but updates the network parameters rather than the joint states. Unlike the implicit solving process discussed above, the NN functions as a forward model that directly maps the input space (P_i) to the output space (τ_i), and is therefore able to make predictions in negligible time once properly trained. In the following sections, we demonstrate how our proposed method solves for the pneumatic gripper gesture when affected by self-weight and holding an object.

Gravity effect

We first examine the proposed gesture predictor under the simple scenario where no object is involved ($N = 0$, $f = 0$). Therefore, the only external factor affecting the soft gripper is gravity. Unlike any rigid gripper whose input signals have absolute control of the gesture, a soft pneumatic gripper's gesture can be heavily affected by its self-weight, especially when operating in a vertical configuration. The predictor's objective is to search for a proper gesture where the gripper's self-weight and the corresponding torque generated are well balanced by the pneumatic joints (Equation 1). We use an initial guess of 0 for the joint force and torque states with a limited memory Broyden-Fletcher-Goldfarb-Shanno (L-BFGS) optimizer, which conducts quasi-Newton method with some stochastic line search to update the joint states τ_i . The solution process takes approximately 2–3 s to converge whereas the FEM approach takes more than 20 min to calculate the entire gesture even when no forces or torques are involved. The predictions are then validated experimentally with the 3D printed pneumatic gripper, as shown in Figure 5A. The middle column of Figure 5A shows the gestures that are directly interpolated from the surrogate model assuming no force or torque interactions. It can be observed that the gripper deforms much more significantly than experiments (left column) if the gravity effect is

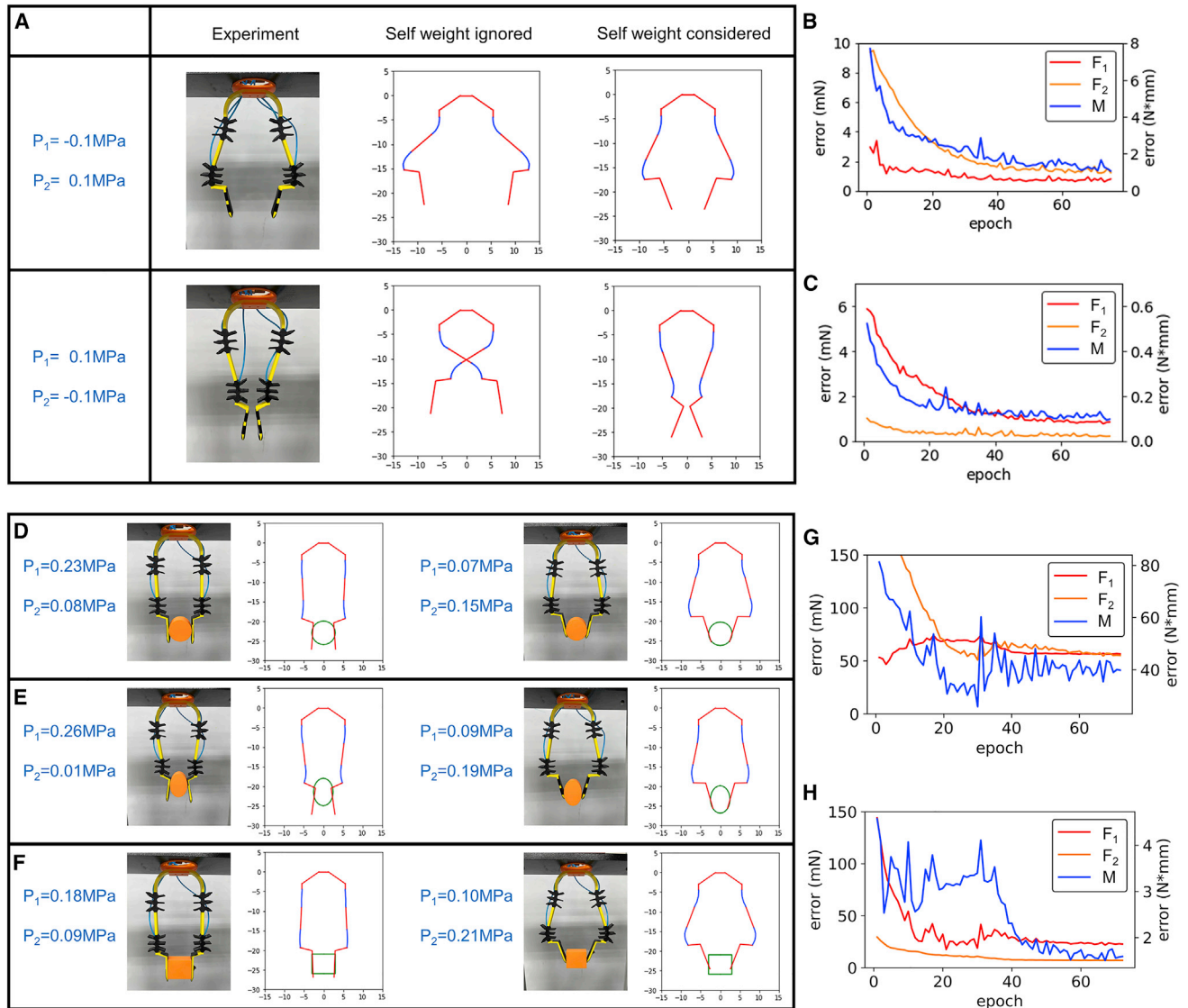


Figure 5. Gesture predictions under pure gravitational effects and when gripping objects

(A–C) (A) Comparison between the gesture predictor and experimental results when there is no object. The experiments are conducted in the vertical plane. For the predicted gesture plots, the red curves represent the rigid components, and the blue curves represent the pneumatic joints. Two different input pressures are investigated with $P_1 = -0.1\text{ MPa}$, $P_2 = 0.1\text{ MPa}$, and $P_1 = 0.1\text{ MPa}$, $P_2 = -0.1\text{ MPa}$. The validation error during the training of an object-free gesture predictor neural network is shown for the averaged unbalanced force and torques at (B) joint 1 over 75 epochs of training and (C) joint 2 over 75 epochs of training.

(D) Two different gestures to hold a circular object (colored as green) which has a radius of 3 cm, and a weight of 0.2 N. The predictions (red curves for rigid components, blue curves for pneumatic joints) are compared with experimental results conducted in the vertical plane.

(E) Two different gestures to hold an elliptical object, which has a major axis of 3.5 cm, a minor axis of 2.5 cm, and a weight of 0.2 N.

(F–H) (F) Two different gestures to hold a rectangular object, which has a length of 6 cm, a height of 5 cm, and a weight of 0.2 N. The validation error during the training of the gesture predictor neural network shown for the averaged unbalanced force and torques at (G) joint 1 over 75 epochs of training and (H) joint 2 over 75 epochs of training.

ignored (self-collision is not considered allowing the gripper fingers to cross each other). The right column shows the converged solutions from the gesture predictor, which matches well with the experimental results on the 3D printed gripper. Small discrepancies can be observed between our predictions and experiments due to pressure gauge resolution, pressure tube stiffness, joint surrogate model uncertainties, and the joint interface assumption (more details in the [discussion](#)).

Furthermore, we test the NN approach to maximize the gesture prediction process efficiency and decrease computational time. As previously discussed, an NN is constructed to take pressure controls P_i as inputs and predict the joint operating states τ_i as outputs. The NN consists of 4 hidden layers with sizes of 32, 64, 64, and 32. Using a uniform distribution, 4,800 sets of input pressures are randomly generated within the range of 0–0.3 MPa, where 4,000 are for training and 800 are for validation. Using the same loss function (Equation 1) as for the implicit gesture predictor, the NN predictor is trained for 75 epochs using the Adam optimizer with a batch size of 20, learning rate of 3×10^{-4} , and exponential rate decay factor of 0.94. The training procedure is accomplished within 10 min on an RTX 2080 GPU. Figures 5B and 5C show the amount of force and torque mismatch at the two joints evaluated on the validation dataset throughout the training procedure. For all predictions from this trained NN predictor, the expected force and torque unbalance is below 2 mN and 1.2 Nmm. The NN predictions are indistinguishable from the implicit predictor solutions and well match the experiments. Furthermore, it takes less than 0.1 s to query this NN model and obtain the gesture prediction (compared with 20–30 min to do the same task using FEM, for example). We note that the NN model can also be realized through a supervised manner where ground truth labels can be obtained first by solving the gestures individually using the implicit predictor. However, such data-based training would be extraneous as the solution process can be integrated into the training loss function.

Object gripping

We have shown that the proposed approach can accurately and efficiently predict the pneumatic gripper gesture under gravity. The next step is to model the object gripping gesture. Specifically, contact forces will be involved. The predictor has the exact same structure as discussed before, but the net force and torque loss functions now contain two additional terms: a normal contact force approximated using the penalty method, and a static friction determined by the object weight and friction cone (the friction coefficient is set to 0.3). The gripper tip is discretized into small segments whose penetration magnitudes are determined from a local contact search (Figure S1). The same L-BFGS optimizer is used to update the force and torque predictions starting from the initial 0-point. However, it is difficult for the optimizer to converge for a couple of reasons: first, the contact penalty term may generate huge gradient steps due to the nonlinear contact boundary and force magnitude. Second, the uncertainty and nonlinearity of the NN joint surrogate model are amplified due to the large contact penalty. Finally, multiple static contact solutions for a soft pneumatic gripper can exist. To resolve the aforementioned issues, we apply extra penalty terms F_1 , F_2 , and M to the loss function whenever these terms exceed their respective thresholds of 3 N, 3 N, and 0.1 Nm. These extra terms help the predictor avoid the domain where the joint surrogate model is not trained on. Moreover, ramp-based intermediate sub-steps are inserted during the solution process to restrict the solution search within the local convex hull. With these modifications applied, the predictor takes approximately 10–15 s to converge depending on the input pressures and the object shape. On the other hand, solving the object gripping gesture through the FEM approach can take over 30 min (more than 100× longer). The predictions are then validated with the 3D printed pneumatic gripper. We test three different object shapes, respectively, as demonstrated in Figures 5D–5F: a circular object with a radius of 30 mm, an elliptical object with a major axis of 35 mm and minor axis of 25 mm, and a rectangular 60 × 50 mm object. Two gestures are demonstrated for each of these objects with different pressure inputs at the pneumatic joints. The predicted object gripping gestures well match the experimental results for all six cases with small discrepancies caused by

pressure gauge resolution, pressure tube stiffness, joint surrogate model uncertainties, and the joint interface assumption (more details in the [discussion](#)).

The NN approach is also examined for object gripping gesture prediction. As a case study, we use a circular object with 30 mm radius, 20 g weight, and 23 cm away from the gripper base. The goal is to train an NN to predict the gripping gesture for this circular object at different input pressures. We adopt the same NN structure and physics-driven training configuration as used for the gravity effect only. However, the NN predictor faces difficulties in learning the object gripping gesture properly. The converged NNs still yield an average net force loss of over 0.01 N and a net torque loss of over 7 Nmm, 10 times higher than the case without contact as plotted in [Figures 5G](#) and [5H](#). Overall, the NNs can make reasonable predictions under small pressure inputs where the gripper tip is not supposed to be in contact with the object ([Figure S2A](#)). However, for large input pressures that force the gripper to interact with the object, the NN tends to make erroneous gesture predictions ([Figure S2B](#)). The difference in predictions is mainly caused by inaccurate gradient directions due to the nonlinearity of static contact evaluation.

DISCUSSION

We have demonstrated that the proposed modeling framework can predict pneumatic gripper gestures in seconds with negligible mismatch. Such fast prediction capability is an important feature for a variety of robotics applications where a large number of gesture trials are needed for better control.^{52–54} Unlike rigid robotic arms, which are governed mostly by linear mechanics, the major difficulty of soft gripper gesture prediction lies in the compliance of its pneumatic components causing nonlinear interaction between the gripper and any external forces. While the FEM approach has been extensively used to predict the deformation of pneumatic actuators,^{55–58} accurate results from FEM come with an expensive computational cost. On the other hand, our iterative predictor can perform the same task 100 times faster than FEM simulations. One key component for realizing such accelerated predictions is the data-driven joint surrogate model, which takes approximately 12 days for data collection and supervised training. This NN model not only allows for fast forward prediction, but more importantly functions as an analytical mechanics model with gradients available for backpropagation. Moreover, the surrogate model can be directly adapted to different finger or gripper configurations without additional precomputation (training) as long as the pneumatic joint articulation remains unchanged. However, the current surrogate model contains two major limitations that cannot be easily overcome with more training data. First, the NN surrogate model is trained to minimize the coordinate error, whereas the joint end slope plays a more critical role in gesture prediction. As shown in [Figure 3](#), error in slope prediction will be amplified over the entire gripper finger, making the gesture prediction more sensitive to the joint end orientation than the centerline coordinates. Second, the first-order derivative of the surrogate model prediction is not regularized during the training process. This can generate undesired gradients that negatively affect the Newton search of the L-BFGS optimizer.⁵⁹ Future work will be dedicated to address these drawbacks by modifying the network structure and training loss function. Another potential improvement for the surrogate model is to obtain ground truth data from experimental images. Therefore, future efforts will include automating the control system and developing image-processing algorithms to extract pneumatic joint deformation from images. Besides the surrogate model, gesture prediction discrepancy also originates from the geometry and mechanics simplifications we made. For instance, our model assumes a tangential connection at the

interface of the pneumatic joints and rigid components, which is not always the case experimentally due to the flexible behavior of the joint end surface. Furthermore, the pin-hole structure used for gripper assembly (Figure S4C) slightly stiffens the end of the pneumatic joints, causing the experimental joint deformation to be smaller than the data collected from FEM. The pneumatic pressurization tubes will also generate resistive forces or torques that impede the deformation of the gripper, which is not considered either in FEM or the proposed method. In the future, these errors can potentially be estimated and compensated for as a function of pressure inputs using a few experimental observations.^{60–62} Despite all the aforementioned sources of error, the gesture predictor is still capable of producing reasonable predictions that are in close agreement with experimental results as seen in Figure 5. One important reason is that all the external forces and torques from gravity or object contact tend to resist the gripper deformation caused by pressure inputs, and therefore reduces the overestimation of gripper deformation.

Although the proposed efficient gesture predictor does accelerate the computation time by orders of magnitude, it still involves an implicit searching process making instantaneous predictions difficult. The NN gesture predictor presented here functions as a forward model and offers an opportunity for real-time soft gripper prediction by making an inference in less than 0.1 s. As discussed in the results, when gravity is the only external factor, the NN predictor can be trained directly using the balance loss at randomly selected pressure inputs. In other words, we can make instantaneous gripper gesture predictions with the joint FEM simulations being the only considerable computation cost (NN training time is significantly shorter than data collection). However, the same approach is not successful when applied to estimate an object gripping gesture as plotted in Figures 5G and 5H. We identify two major reasons causing this to happen. First, the normal contact force calculated through the penalty method is much more sensitive to the gripper tip displacement than gravity as seen in Figure S3. Unlike the smooth torque change caused by gravity, the normal contact force starts to generate excessive amounts of torque on the gripper tip as the amount of penetration increases. This phenomenon causes the NN to favor gestures that are free of contact forces since the goal of NN training is to minimize the expected loss from batches of data. However, decreasing the contact coefficient further would cause unrealistic results as we can already observe small overlaps between the object and gripper tip (Figure 5). Second, considering the nonlinear behavior of pneumatic joints, the solution to a static contact problem is not only a function of the final pressure inputs but also the pressure history. This history dependence is considered in the iterative predictor by adding intermediate sub-steps so that the pressure increment is small enough to avoid multiple local minima. However, the NN is not structured to take the pressure history into account, and therefore fails to converge to the correct mapping between the pressure inputs and the gestures. This further suggests that the current pressure states alone are inadequate for the NN input space, since they do not uniquely determine the gripping gesture. Potential solutions to this NN behavior will be explored in future work, including the possibility of remapping the contact normal force to smooth out the loss function and using recurrent NNs to make incremental gesture predictions. Note that only two solutions are demonstrated for each object in Figures 5D–5F as they are the most representative gestures that hold the objects stably in experiments. In other words, most reliable grasping gestures are generated by pressure combinations within close neighbors of the presented solutions, and thus look similar to the demonstrated gestures. Nevertheless, one potential application of our predictor is to explore any possible irregular gestures in a simulated environment. The model presented in this work is restricted to the 2D vertical plane.

However, the proposed hybrid gripper prediction framework can be easily extended to general 3D scenarios with a couple of modifications. For instance, all position vectors will have one more degree of freedom, the loading vector will have three more degrees of freedom considering out of plane forces and torques, the orientation representations and rotation operations will include one more angle variable, and the friction cone will become a 2D region. Moreover, future work will include design and modeling of a torsional pneumatic joint which is required for adjusting the contact orientation in 3D gripping applications.

EXPERIMENTAL PROCEDURES

Resource availability

Lead contact

Further information is available from the lead contact, Grace X. Gu (ggu@berkeley.edu).

Materials availability

This study did not generate new unique materials.

Data and code availability

All data supporting this study are available in this article and in the [supplemental information](#).

3D printing

All the gripper components, including the pneumatic joints and the rigid parts (Figures S4A and S4B), are 3D printed using the Prusa i3 MK3S fused filament fabrication (FFF) printer. A 0.4 mm nozzle is used in this study with a layer height of 0.2 mm. All the rigid gripper components are printed from polylactic acid (PLA) filaments at 20% infill density, 65°C bed temperature, 215°C nozzle temperature, and 60 mm/s infill printing speed. The pneumatic joints are printed from NinjaFlex (a type of thermoplastic polyurethane) filaments at 100% infill density, 80 °C bed temperature, 240°C nozzle temperature, and 15 mm/s infill printing speed. The pneumatic joint is designed such that its pressure channels fully utilize the bridging ability of the FFF printer and require zero support structure. The bellow has a wall thickness of 1.2 mm (equivalent to three rasters), the minimum requirement to ensure air tightness. Each joint takes approximately 4 h to be printed. The weight of the 3D printed pneumatic joint, rigid link, and rigid tip are measured to be 0.09, 0.04, and 0.06 N, respectively, and these weights are used in Equation 1 to model gravity's effect on the gripper gesture. Using the pin-hole structures as seen in Figure S4C, the printed components are then assembled into the gripper with a tip opening distance of 5 cm at free state. However, the gripper can handle objects that are slightly wider than 5 cm utilizing the bidirectional bending ability of the pneumatic joints. The three sample objects shown in Figures 5D–5F are also 3D printed using PLA filaments. The infill density is adjusted so that all three objects share the same weight of 0.2 N and surface friction coefficient of 0.3.

Pressure control

Each pneumatic joint contains two pressure channels controlled independently so that the joints can bend in different directions. Since the two channels are never pressurized simultaneously, we represent the pressure state of each pneumatic joint with only one parameter whose plus or minus sign corresponds to the top or bottom channel (Figure 1C), respectively. The entire gripper consists of four pneumatic joints leading to eight pressure channels controlled by four pressure regulators based on symmetry. The pressure regulator has a resolution of 0.01 MPa. For each

experimental test, the gestures are recorded at least 2 min after full pressurization to ensure static conditions and avoid any creep behavior at the pneumatic joints. Pressure channels of the pneumatic joints can endure a maximum pressure of 0.6 MPa before leaking, which corresponds to a maximum gripping weight of approximately 250 g.

Tensile test

Material properties of NinjaFlex are characterized through uniaxial quasi-static tensile tests (see Note S2). Three NinjaFlex dogbones are 3D printed with their gauge length labeled by white marks (Figure S5A). The dogbones are extended by 40 mm at a rate of 3 mm/min to avoid any viscoelastic behavior. Engineering strain is calculated as the percentage change of the gauge length and converted to true strain by taking the natural log. True stress is obtained by assuming constant volumes of the dogbone specimens. Figure S5B shows the averaged stress-strain plot of the three dogbone specimens. The stress-strain plot is highly linear up to a true strain of 0.8, which can be fully captured by a linear elastic material model with a Young's modulus of 12.2 MPa. Considering NinjaFlex is a typical thermoplastic polyurethane material and is virtually incompressible, the Poisson's ratio is set to 0.49.^{63,64}

Finite element analysis

Finite element analysis is performed using an ANSYS static structural module to obtain the deformation of pneumatic gripper under different loading conditions with large deflection enabled. Based on symmetry, only half of the pneumatic joint (split from the cross-section plane as shown in Figure 1C) is analyzed. The contacts between the inner walls of the pressure channels are assumed to be frictionless. We adopt a tetrahedron mesh with an element size of 1.2 mm over the entire geometry. The element size is chosen to balance the accuracy and computation cost. Further decreasing the element size from 1.2 to 1.0 mm causes less than 3% change in displacements but increases the number of nodes from 16,000 to 23,000. The boundary condition includes zero displacement at the left end and zero normal displacement at the symmetry plane. The loading condition includes pressure at the two channels, normal (F_1) and shear (F_2) forces, as well as a torque applied to the right end of the gripper. The maximum equivalent strain under most loading cases does not exceed 0.4, which means that the linear elastic material model is well qualified for this study. On average, each pneumatic joint simulation takes approximately 6–7 min to complete on an Intel Xeon E-2146 CPU.

SUPPLEMENTAL INFORMATION

Supplemental information can be found online at <https://doi.org/10.1016/j.xcrp.2022.100842>.

ACKNOWLEDGMENTS

The authors acknowledge support from Amazon, Johnson & Johnson, and the Hellman Fellows Program. In addition, the authors acknowledge support from the Extreme Science and Engineering Discovery Environment (XSEDE) by the National Science Foundation grant no. ACI-1548562.

AUTHOR CONTRIBUTIONS

Z.Z. and G.X.G. conceived the project. Z.Z. and Z.J. conducted finite element analysis for the pneumatic gripper. Z.J. trained the neural network surrogate model for the pneumatic joint. Z.Z. developed the gesture prediction algorithm based on the joint surrogate model. Z.Z. and Z.J. 3D printed the pneumatic gripper and

experimentally validated the prediction results. G.X.G. supervised the model training, predictor algorithm development, experiments, and data analysis. All authors contributed to the writing and revisions.

DECLARATION OF INTERESTS

The authors declare no competing interests.

Received: December 28, 2021

Revised: March 7, 2022

Accepted: March 14, 2022

Published: April 4, 2022

REFERENCES

- Laschi, C., and Cianchetti, M. (2014). Soft robotics: new perspectives for robot bodyware and control. *Front. Bioeng. Biotechnol.* 2, 3.
- Alici, G. (2018). Softer is harder: what differentiates soft robotics from hard robotics? *MRS Adv.* 3, 1557–1568.
- Rus, D., and Tolley, M.T. (2015). Design, fabrication and control of soft robots. *Nature* 521, 467–475.
- Ben-Ari, M., and Mondada, F. (2017). *Elements of Robotics* (Springer Nature).
- Whitesides, G.M. (2018). Soft robotics. *Angew. Chem. Int. Ed.* 57, 4258–4273.
- Albu-Schaffer, A., Eiberger, O., Grebenstein, M., Haddadin, S., Ott, C., Wimbock, T., Wolf, S., and Hirzinger, G. (2008). Soft robotics. *IEEE Robotics Automation Mag.* 15, 20–30.
- Mazzolai, B., Margheri, L., Cianchetti, M., Dario, P., and Laschi, C. (2012). Soft-robotic arm inspired by the octopus: II. From artificial requirements to innovative technological solutions. *Bioinspir. Biomim.* 7, 025005.
- Pfeifer, R., Lungarella, M., and Iida, F. (2012). The challenges ahead for bio-inspired/soft robotics. *Commun. ACM* 55, 76–87.
- Di Lallo, A., Yu, S., Huang, T.-H., Bulea, T.C., and Su, H. (2021). High-performance soft wearable robots for human augmentation and gait rehabilitation. In *Soft Robotics in Rehabilitation* (Elsevier), pp. 1–38.
- Wang, Z., Chathuranga, D.S., and Hirai, S. (2016). 3D Printed Soft Gripper for Automatic Lunch Box Packing (IEEE), pp. 503–508.
- Laschi, C., Rossiter, J., Iida, F., Cianchetti, M., and Margheri, L. (2017). *Soft Robotics: Trends, Applications and Challenges* (Springer).
- Giorgio-Serchi, F., and Weymouth, G.D. (2017). Underwater soft robotics, the benefit of body-shape variations in aquatic propulsion. In *Soft Robotics: Trends, Applications and Challenges* (Springer), pp. 37–46.
- Fras, J., and Althoefer, K. (2018). *Soft Biomimetic Prosthetic Hand: Design, Manufacturing and Preliminary Examination* (IEEE), pp. 1–6.
- Yamada, K., Takuma, T., and Kase, W. (2019). Hydraulic-driven Soft Robot for Entering into Small Gap Fed by Indirect Information of Contacting State (IEEE), pp. 1933–1940.
- Talas, S.K., Baydere, B.A., Altinsoy, T., Tutcu, C., and Samur, E. (2020). Design and development of a growing pneumatic soft robot. *Soft robotics* 7, 521–533.
- Renda, F., Giorelli, M., Calisti, M., Cianchetti, M., and Laschi, C. (2014). Dynamic model of a multibending soft robot arm driven by cables. *IEEE Trans. Robotics* 30, 1109–1122.
- Kastor, N., Mukherjee, R., Cohen, E., Vikas, V., Trimmer, B.A., and White, R.D. (2020). Design and manufacturing of tendon-driven soft foam robots. *Robotica* 38, 88–105.
- Laschi, C., Cianchetti, M., Mazzolai, B., Margheri, L., Follador, M., and Dario, P. (2012). Soft robot arm inspired by the octopus. *Adv. robotics* 26, 709–727.
- Anderson, I.A., Gisby, T.A., McKay, T.G., O'Brien, B.M., and Calius, E.P. (2012). Multi-functional dielectric elastomer artificial muscles for soft and smart machines. *J. Appl. Phys.* 112, 041101.
- Pelrine, R., Kornbluh, R., Pei, Q., and Joseph, J. (2000). High-speed electrically actuated elastomers with strain greater than 100%. *Science* 287, 836–839.
- Yap, Y.L., Sing, S.L., and Yeong, W.Y. (2020). A review of 3D printing processes and materials for soft robotics. *Rapid Prototyping J.* 26, 1345–1361.
- Keong, B.A.W., and Hua, R.Y.C. (2018). A novel fold-based design approach toward printable soft robotics using flexible 3D printing materials. *Adv. Mater. Tech.* 3, 1700172.
- Wilt, J.K., Yang, C., and Gu, G.X. (2020). Accelerating auxetic metamaterial design with deep learning. *Adv. Eng. Mater.* 22, 1901266.
- Manti, M., Hassan, T., Passetti, G., D'Elia, N., Laschi, C., and Cianchetti, M. (2015). A bioinspired soft robotic gripper for adaptable and effective grasping. *Soft Robotics* 2, 107–116.
- Tyagi, M., Pan, J., and Jager, E.W. (2019). Novel fabrication of soft microactuators with morphological computing using soft lithography. *Microsyst. nanoeng.* 5, 1–10.
- Zhang, Z., Demir, K.G., and Gu, G.X. (2019). Developments in 4D-printing: a review on current smart materials, technologies, and applications. *Int. J. Smart Nano Mater.* 10, 205–224.
- Todorov, E., Erez, T., and Tassa, Y. (2012). Mujoco: A Physics Engine for Model-Based Control (IEEE), pp. 5026–5033.
- Erez, T., Tassa, Y., and Todorov, E. (2015). Simulation Tools for Model-Based Robotics: Comparison of Bullet, Havok, Mujoco, Ode and Physx (IEEE), pp. 4397–4404.
- Todorov, E. (2014). Convex and Analytically-Invertible Dynamics with Contacts and Constraints: Theory and Implementation in Mujoco (IEEE), pp. 6054–6061.
- Koenemann, J., Del Prete, A., Tassa, Y., Todorov, E., Stasse, O., Bennewitz, M., and Mansard, N. (2015). Whole-body Model-Predictive Control Applied to the HRP-2 Humanoid (IEEE), pp. 3346–3351.
- Tassa, Y., Erez, T., and Todorov, E. (2012). Synthesis and Stabilization of Complex Behaviors through Online Trajectory Optimization (IEEE), pp. 4906–4913.
- Mosadegh, B., Polygerinos, P., Keplinger, C., Wennstedt, S., Shepherd, R.F., Gupta, U., Shim, J., Bertoldi, K., Walsh, C.J., and Whitesides, G.M. (2014). Pneumatic networks for soft robotics that actuate rapidly. *Adv. Funct. Mater.* 24, 2163–2170.
- Hu, W., Mutlu, R., Li, W., and Alici, G. (2018). A structural optimisation method for a soft pneumatic actuator. *robotics* 7, 24.
- Demir, K.G., Zhang, Z., Yang, J., and Gu, G.X. (2020). Computational and experimental design exploration of 3D-printed soft pneumatic actuators. *Adv. Intell. Syst.* 2, 2000013.
- Webster, R.J., III, and Jones, B.A. (2010). Design and kinematic modeling of constant curvature continuum robots: a review. *Int. J. Robotics Res.* 29, 1661–1683.
- Chen, Y., Wang, L., Galloway, K., Godage, I., Simaan, N., and Barth, E. (2021). Modal-based kinematics and contact detection of soft robots. *Soft Robotics* 8, 298–309.
- Mohamed, M.H., Wagdy, S.H., Atalla, M.A., Rehan Youssef, A., and Maged, S.A. (2020). A proposed soft pneumatic actuator control based on angle estimation from data-driven model. *Proc. Inst. Mech. Eng. H.* 234, 612–625.

38. Deimel, R., and Brock, O. (2013). A Compliant Hand Based on a Novel Pneumatic Actuator (IEEE), pp. 2047–2053.
39. Robertson, M.A., Sadeghi, H., Florez, J.M., and Paik, J. (2017). Soft pneumatic actuator fascicles for high force and reliability. *Soft robotics* 4, 23–32.
40. Hao, Y., Gong, Z., Xie, Z., Guan, S., Yang, X., Ren, Z., Wang, T., and Wen, L. (2016). Universal Soft Pneumatic Robotic Gripper with Variable Effective Length (IEEE), pp. 6109–6114.
41. Chen, C.-T., and Gu, G.X. (2021). Learning hidden elasticity with deep neural networks. *Proc. Natl. Acad. Sci. U S A* 118, e2102721118.
42. Yan, S., Zou, X., Ilkhani, M., and Jones, A. (2020). An efficient multiscale surrogate modelling framework for composite materials considering progressive damage based on artificial neural networks. *Composites B: Eng.* 194, 108014.
43. Jin, Z., Zhang, Z., Demir, K., and Gu, G.X. (2020). Machine learning for advanced additive manufacturing. *Matter* 3, 1541–1556.
44. Gongora, A.E., Xu, B., Perry, W., Okoye, C., Riley, P., Reyes, K.G., Morgan, E.F., and Brown, K.A. (2020). A Bayesian experimental autonomous researcher for mechanical design. *Sci. Adv.* 6, eaaz1708.
45. Kim, B., Lee, S., and Kim, J. (2020). Inverse design of porous materials using artificial neural networks. *Sci. Adv.* 6, eaax9324.
46. Jin, Z., Zhang, Z., Ott, J., and Gu, G.X. (2021). Precise localization and semantic segmentation detection of printing conditions in fused filament fabrication technologies using machine learning. *Additive Manufacturing* 37, 101696.
47. Hanakata, P.Z., Cubuk, E.D., Campbell, D.K., and Park, H.S. (2020). Forward and inverse design of kirigami via supervised autoencoder. *Phys. Rev. Res.* 2, 042006.
48. Minh Nguyen-Thanh, V., Trong Khiem Nguyen, L., Rabczuk, T., and Zhuang, X. (2020). A surrogate model for computational homogenization of elastostatics at finite strain using high-dimensional model representation-based neural network. *Int. J. Numer. Methods Eng.* 121, 4811–4842.
49. Zhang, Z., and Gu, G.X. (2021). Physics-informed deep learning for digital materials. *Theor. Appl. Mech. Lett.* 11, 100220.
50. Pandey, A., and Pokharel, R. (2021). Machine learning based surrogate modeling approach for mapping crystal deformation in three dimensions. *Scripta Materialia* 193, 1–5.
51. Zhang, Z., and Gu, G.X. (2020). Finite-element-based deep-learning model for deformation behavior of digital materials. *Adv. Theor. Simulations* 3, 2000031.
52. Körber, M., Lange, J., Rediske, S., Steinmann, S., and Glück, R. (2021). Comparing popular simulation environments in the scope of robotics and reinforcement learning. Preprint at arXiv. <https://doi.org/10.48550/arXiv.2103.04616>.
53. Yuan, W., Hang, K., Kragic, D., Wang, M.Y., and Stork, J.A. (2019). End-to-end nonprehensile rearrangement with deep reinforcement learning and simulation-to-reality transfer. *Robotics Autonomous Syst.* 119, 119–134.
54. Benatti, S., Tasora, A., Fusai, D., and Mangoni, D. (2019). A Modular Simulation Platform for Training Robots via Deep Reinforcement Learning and Multibody Dynamics (ICACR 2019), pp. 7–11.
55. Rehman, T., Dewi, D.E.O., and Ali, M.S.M. (2017). Finite Element Analysis for PDMS Based Dual Chamber Bellows Structured Pneumatic Actuator (Springer), pp. 392–402.
56. Zolfagharian, A., Durran, L., Gharai, S., Rolfe, B., Kaynak, A., and Bodaghi, M. (2021). 4D printing soft robots guided by machine learning and finite element models. *Sensors Actuators A: Phys.* 328, 112774.
57. Hassan, T., Cianchetti, M., Moatamedi, M., Mazzolai, B., Laschi, C., and Dario, P. (2018). Finite-element modeling and design of a pneumatic braided muscle actuator with multifunctional capabilities. *IEEE/ASME Trans. Mechatronics* 24, 109–119.
58. Tawk, C., and Alici, G. (2020). Finite element modeling in the design process of 3D printed pneumatic soft actuators and sensors. *Robotics* 9, 52.
59. Berahas, A.S., Nocedal, J., and Takáč, M. (2016). A Multi-Batch L-BFGS Method for Machine Learning. Preprint at arXiv. <https://doi.org/10.48550/arXiv.1605.06049>.
60. Woodacre, J., Bauer, R., and Irani, R. (2018). Hydraulic valve-based active-heave compensation using a model-predictive controller with non-linear valve compensations. *Ocean Eng.* 152, 47–56.
61. Li, Y., Chen, J., and Lan, F. (2020). Enhanced online model identification and state of charge estimation for lithium-ion battery under noise corrupted measurements by bias compensation recursive least squares. *J. Power Sourc.* 456, 227984.
62. Zou, P., Zhu, Q., Wu, J., and Jin, J. (2019). An Approach for Peg-In-Hole Assembling Based on Force Feedback Control (IEEE), pp. 3269–3273.
63. Pagac, M., Schwarz, D., Petru, J., and Polzer, S. (2020). 3D printed polyurethane exhibits isotropic elastic behavior despite its anisotropic surface. *Rapid Prototyping J.* 26, 1371–1378.
64. Qi, H.J., and Boyce, M.C. (2005). Stress-strain behavior of thermoplastic polyurethanes. *Mech. Mater.* 37, 817–839.